Birefringence and Depolarized Light Scattering of an Ordered Block Copolymer Melt under Shear Flow

H. Wang, M. C. Newstein, M. Y. Chang, N. P. Balsara,*,† and B. A. Garetz*,†

Department of Chemical Engineering, Chemistry and Materials Science, and Department of Electrical Engineering, Polytechnic University, Six Metrotech Center, Brooklyn, New York 11201

Received November 24, 1999

ABSTRACT: A combination of in situ birefringence and depolarized light-scattering experiments was used to study the formation of an ordered cylindrical microstructure in a polystyrene-*block*-polyisoprene copolymer melt under a shear flow field. We demonstrate that our sample forms an imperfect "single crystal" with a fraction of the cylinders aligned in the flow direction. The aligned regions of the sample coexist with randomly oriented grains. The birefringence experiments enable the characterization of the aligned regions while the depolarized light-scattering experiments enable the characterization of the randomly oriented grains. A model for depolarized light scattering from such samples was developed. It was shown that the usual scattering formulas for grains embedded in an isotropic matrix are applicable provided one recognizes that the scattering vector, $\mathbf{q}$, has transverse ($\mathbf{q}_T$) and longitudinal ($\mathbf{q}_L$) components even in the small angle scattering limit ($\mathbf{q}_L$ is the component of $\mathbf{q}$ in the propagation direction). This result applies when the analyzer (or polarizer) axis is aligned along the direction of the optic axis of the aligned regions. A simplifying feature of block copolymers is that the product $w|\mathbf{q}_L| \ll 1$, where w is the characteristic grain size, allowing the approximation $\mathbf{q} \approx \mathbf{q}_T$. We used our model to study the structure of the block copolymer melt after it had been quenched from the disordered to the ordered state under reciprocating shear flow (strain amplitude = 133%). Under slow shear flow (shear rate, $\dot{\gamma} = 0.067\ s^{-1}$), about 60% of the sample consisted of randomly oriented grains and 40% consisted of aligned cylinders. The average grain size and time required to complete the ordering process obtained under slow shear flow were comparable to those obtained under quiescent conditions. Under fast shear flow ($\dot{\gamma} = 0.67\ s^{-1}$), however, most of the sample (97%) consisted of aligned cylinders, indicating the formation of a well-aligned crystal.

Introduction

Hierarchical organization is often found in crystalline and liquid-crystalline polymer materials.[1−3] On molecular length scales, semicrystalline polymer chains form lamellae, rodlike polymers exhibit nematic order, and block copolymer molecules form ordered structures such as cylinders arranged on a hexagonal lattice. These molecular structures are, in turn, organized into domains which are of supramolecular length scales. The orientation of the molecular structures is correlated within these domains. In semicrystalline polymers (Figure 1a), the lamellar crystals are organized in a radial arrangement and the domains are called spherulites. In samples with liquid crystalline order (Figure 1b,c), the domains are regions within which the local directors are coherently aligned. An interesting feature of these systems is that the typical length scales of the domains, obtained when the materials are ordered under quiescent conditions, range between 1 and 10 μm, regardless of chemical structure. Consequently, the optical properties of widely different materials such as crystalline polyethylene, solutions of rodlike polymers such as poly(benzylglutamate), and melts of diblock copolymer such as polystyrene-*b*-polyisoprene (both blocks are amorphous) share many common features.[1−14]

In the absence of external fields, the materials are isotropic and the domains are randomly oriented (Figure 1). In many applications, however, the domain structure of polymer materials is aligned by the imposition of flow fields.[5,9−29] For example, the remarkable strength-to-cost ratio of polyethylene films is due, in part, to optimized flow and thermal treatment during processing which leads to a highly anisotropic microstructure.[30] Similarly, ultrastrong polymer fibers used in space and medical applications are made by imposing extensional flow on liquids composed of stiff polymer molecules such as Kevlar.[31] Recent efforts to use block copolymers in electronic and photonic devices[32,33] require the production of single crystals. Several researchers have demonstrated that this can be achieved by the application of flow fields.[5,15−29]

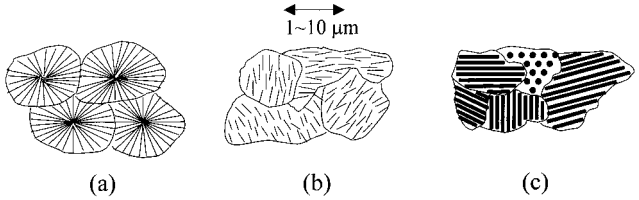

Figure 1. Schematic view of hierarchical organization in polymers with (a) crystalline and (b, c) liquid crystalline symmetry. (a) Crystalline spherulites with radially arranged lamellae. (b) Rodlike polymers with nematic order. (c) Block copolymer with cylinders arranged on a hexagonal lattice. In all cases, the size of the coherently ordered domains is usually in the 1−10 μm range.

Optical techniques are often used to study the flow alignment of polymer microstructure. Keller et al. used birefringence measurements to demonstrate the dramatic alignment of block copolymer cylinders after extrusion.[5] Similar techniques have been used to study solutions of rodlike polymers and block copolymers.[4,6,9,12,13,18] In these studies, the transmitted light intensity is related to microstructure, assuming that the

† Department of Chemical Engineering, Chemistry and Materials Science, Polytechnic University.

10.1021/ma991982z CCC: $19.00
Published on Web 04/21/2000

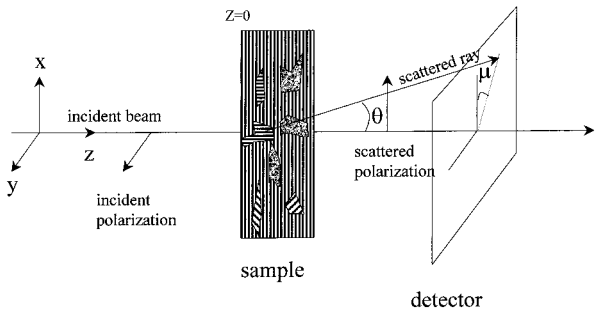

Figure 2. Schematic of the sample and scattering geometry. The striped background in the sample represents the aligned cylinders, the small striped regions represent randomly oriented grains, and the small gray regions represent disordered regions in the sample.

sample is a "single crystal". On the other hand, depolarized light-scattering measurements under shear and tensile fields have been used to characterize domain structure in crystalline polymers and solutions of rodlike polymers.[10,11,14] It has been recognized that analysis of scattering data from deformed samples requires accounting for the polarization changes in the incident and scattered beams as they propagate through the birefringent medium.[10,11] However, in many cases, this effect is ignored, and the scattering profiles are analyzed on the basis of models developed for isotropic systems (e.g., ref 14). Specific criteria for judging the importance of the nonisotropic background do not exist. While Stein and co-workers have obtained solutions for some specific systems,[10,11] a unified framework for analyzing scattering profiles from macroscopically aligned systems does not exist.

In this paper, we develop a model for light scattering from partially aligned systems. We consider a collection of randomly arranged uniaxial grains and disordered regions embedded in a uniaxial, aligned crystal; see Figure 2. The structure in our system can be studied by two separate experiments:

(1) The random grain structure can be probed by depolarized light scattering, if the polarization of the incident or scattered beam is perpendicular to the optic axis of the single crystal. In such an experiment, both the incident and orthogonally polarized scattered light beams propagate without a change in the polarization state. Even in this case, the presence of the birefringent medium cannot be ignored because the incident and scattered beams propagate at different velocities. We derive a simple expression to account for this effect.

(2) The properties of the aligned crystal can be probed by a birefringence measurement by studying the transmission of a linearly polarized beam at an angle of 45 ° to the optic axis of the single crystal. In the single scattering limit, the fraction of light that is scattered is small and most of the measured transmitted signal is due to the birefringence of the aligned crystal. The analysis of such data is well-known.[34]

We constructed an instrument that enables depolarized light-scattering measurements from samples aligned under shear flow. We used this instrument to conduct both depolarized light-scattering and birefringence measurements on a polystyrene−polyisoprene block copolymer melt.

Theoretical Analysis

We develop a model for depolarized light scattering from a partially ordered block copolymer sample under shear flow, shown in Figure 2. We take the incident beam to be *y*-polarized and directed along the *z* axis. We restrict our attention to uniaxial ordered structures such as lamellae or cylinders packed on a hexagonal lattice. The sample consists of nonoverlapping birefringent (ordered) and nonbirefringent (disordered) regions. The optical properties of the birefringent regions are described by a tensor permittivity, $\overleftrightarrow{\epsilon}(\mathbf{r})$, while those of the nonbirefringent regions are described by a scalar permittivity, ϵ_{scalar}. We assume that the shear flow causes the optic axis of some of the ordered regions to align in the *x* direction. In Figure 2 we show a particular case where the aligned regions are merged into a "single crystal matrix". The remainder of the ordered regions have randomly oriented optic axes. We use the term grains to refer to the collection of the randomly oriented, ordered regions. Thus, the sample permittivity can be expressed as

$$\overleftrightarrow{\epsilon}(\mathbf{r}) = \epsilon_{\text{scalar}}\overleftrightarrow{I}F_{\text{disorder}}(\mathbf{r}) + \overleftrightarrow{\epsilon}_{\text{aligned}}F_{\text{aligned}}(\mathbf{r}) + \sum_j \overleftrightarrow{\epsilon}_j f_j(\mathbf{r}) \quad (1)$$

where $\overleftrightarrow{\epsilon}_{\text{aligned}}$ is the permittivity of the aligned regions (which may or may not be contiguous), $\overleftrightarrow{I}$ is the identity matrix, and $\overleftrightarrow{\epsilon}_j$ is the permittivity of the *j*th randomly oriented region or grain. $F_{\text{disorder}}(\mathbf{r})$, $F_{\text{aligned}}(\mathbf{r})$, are the shape functions of the disordered and aligned regions, respectively, equal to unity if the point $\mathbf{r}$ is in the region and zero otherwise. The shape function of the *j*th random grain is $f_j(\mathbf{r})$. The aligned region is uniform in its optical properties, with permittivity given by

$$\overleftrightarrow{\epsilon}_{\text{aligned}} = \epsilon_0\begin{pmatrix} n_e^2 & 0 & 0 \\ 0 & n_o^2 & 0 \\ 0 & 0 & n_o^2 \end{pmatrix} \quad (2)$$

where n_o and n_e are the ordinary and extraordinary refractive indices, and ϵ_0 is the permittivity of vacuum. If we take $\mathbf{g}_j$ to be a unit vector in the direction of the optic axis of the *j*th grain, and $\{\mathbf{a}_j, \mathbf{b}_j, \mathbf{g}_j\}$ to constitute an orthogonal set of unit vectors, then the dyadic representation of the permittivity of the *j*th grain is given by

$$\overleftrightarrow{\epsilon}_j = \epsilon_0(n_o^2(\mathbf{a}_j\mathbf{a}_j + \mathbf{b}_j\mathbf{b}_j) + n_e^2\,\mathbf{g}_j\mathbf{g}_j) \quad (3)$$

We assume that the scalar permittivity is equal to $\langle\epsilon_{\text{random}}\rangle$, the average of $\overleftrightarrow{\epsilon}_j$ over all orientations, given by

$$\epsilon_{\text{scalar}} = \langle\epsilon_{\text{random}}\rangle = \epsilon_0\frac{2n_o^2 + n_e^2}{3} \quad (4)$$

The difference, $\overleftrightarrow{\delta\epsilon}_j$, between $\overleftrightarrow{\epsilon}_j$ and $\langle\epsilon_{\text{random}}\rangle$ is

$$\overleftrightarrow{\delta\epsilon}_j(\mathbf{r}) = \overleftrightarrow{\epsilon}_j(\mathbf{r}) - \langle\epsilon_{\text{random}}\rangle\overleftrightarrow{I} = \epsilon_0(n_e^2 - n_o^2)\left(\mathbf{g}_j\mathbf{g}_j - \frac{1}{3}\overleftrightarrow{I}\right) \approx 2\epsilon_0 n_o(n_e - n_o)\left(\mathbf{g}_j\mathbf{g}_j - \frac{1}{3}\overleftrightarrow{I}\right) \quad (5)$$

We assume that the spatial distribution of disordered, aligned, granular material in any macroscopic volume of the sample is uniform. The depolarized light scattering from our sample is then not sensitive to the detailed arrangement of the aligned, disordered, or granular

regions in the sample. This allows us to express $\vec{\vec{\epsilon}}(\mathbf{r})$ in terms of the volume fractions of disordered material (ϕ_{disorder}), randomly oriented grains (ϕ_{grains}), and aligned material (ϕ_{aligned})

$$\vec{\vec{\epsilon}}(\mathbf{r}) = (\vec{\vec{I}}\,\langle\epsilon_{\text{random}}\rangle\,(\phi_{\text{disorder}} + \phi_{\text{grains}}) + \vec{\vec{\epsilon}}_{\text{aligned}}\,\phi_{\text{aligned}})F_{\text{sample}}(\mathbf{r}) + \sum_j \vec{\vec{\delta\epsilon}}_j\, f_j(\mathbf{r}) \quad (6)$$

where F_{sample} is the shape function of the whole sample ($F_{\text{sample}} = F_{\text{disorder}} + F_{\text{aligned}} + \sum_j f_j$), and $\phi_{\text{disorder}} + \phi_{\text{grains}} + \phi_{\text{aligned}} = 1$.

The wave equation for the scattered field, **E**, can be written as

$$-\nabla\times\nabla\times\boldsymbol{E} + \frac{{k_0}^2}{\epsilon_0}F_{\text{sample}}(\mathbf{r})(\vec{\vec{I}}\,\langle\epsilon_{\text{random}}\rangle(\phi_{\text{disorder}} + \phi_{\text{grains}}) + \vec{\vec{\epsilon}}_{\text{aligned}}\,\phi_{\text{aligned}})\cdot\boldsymbol{E} = -\frac{{k_0}^2}{\epsilon_0}\sum_j \vec{\vec{\delta\epsilon}}_j\, f_j(\mathbf{r})\cdot\boldsymbol{E} \quad (7)$$

In the limit of weak birefringence, $|n_e - n_o| \ll n_o$, the Born approximation can be used to compute the scattered field, **E**(**r**). We obtain:[7,34,35]

$$\mathbf{E}(\mathbf{r}) = -\frac{{k_0}^2}{\epsilon_0}\int_V \mathrm{d}\mathbf{r}'\,\vec{\vec{G}}(\mathbf{r}-\mathbf{r}')\sum_j \vec{\vec{\delta\epsilon}}_j(\mathbf{r}')f_j(\mathbf{r}')\cdot\mathbf{E}_{\text{incident}}(\mathbf{r}') \quad (8)$$

where $\vec{\vec{G}}(\mathbf{r}-\mathbf{r}')$ is the Green's function dyadic. The incident field, $\mathbf{E}_{\text{incident}}$, is given by $\mathbf{a}_y E_{\text{inc}}\exp(ik_{\text{incident}}z)$ where E_{inc} is its amplitude at $z = 0$, the entrance face of the sample, $\mathbf{a}_y$ is a unit vector in the y direction, and $i = \sqrt{-1}$. The incident wavevector, k_{incident}, is related to the free space wave vector, k_0 ($k_0 = 2\pi/\lambda$, where λ is the wavelength of the incident laser beam in air), by

$${k_{\text{incident}}}^2 = {k_0}^2\left[{n_o}^2 + \frac{1}{3}(\phi_{\text{aligned}} - 1)({n_o}^2 - {n_e}^2)\right] \quad (9)$$

The expression for ${k_{\text{incident}}}^2$ (eq 9) is obtained by substitution of $\mathbf{E}_{\text{incident}}$ into the homogeneous equation obtained by setting the right-hand side of eq 7 equal to zero.

Since the x component of the scattered field maintains its sense of polarization as it propagates through the sample at small scattering angles, we need only the xx component of the Green's function dyadic, which, in the far field limit ($r \gg r'$), has a well-known form

$$G_{xx}(\mathbf{r}-\mathbf{r}') = \frac{\exp(ik_{\text{scattered}}|\boldsymbol{r}-\boldsymbol{r}'|)}{4\pi|\boldsymbol{r}-\boldsymbol{r}'|} \xrightarrow{r\gg r'} -\frac{1}{4\pi r}\exp(ik_{\text{scattered}}r)\exp(-ik_{\text{scattered}}\boldsymbol{r}'\cdot\boldsymbol{s}) \quad (10)$$

where

$${k_{\text{scattered}}}^2 = {k_0}^2\left({n_e}^2 + \frac{2}{3}(\phi_{\text{aligned}} - 1)({n_e}^2 - {n_o}^2)\right) \quad (11)$$

and **s** is a unit vector in the direction of the scattered wave. The expression for ${k_{\text{scattered}}}^2$ (eq 11) is obtained by substitution of $\mathbf{E}_{\text{scattered}} = \mathbf{a}_x E_{\text{scattered}}\exp(ik_{\text{scattered}}z)$ into the homogeneous equation obtained by setting the right-hand side of eq 7 equal to zero.

The x component of the scattered field, $E_x(\mathbf{r})$ is thus obtained by substituting eqs 9, 10, and 11 into eq 8:

$$E_x(\boldsymbol{r}) = \frac{E_{\text{inc}}{k_0}^2}{4\pi r}\exp(ik_{\text{scattered}}r)\times\int_V \mathrm{d}\boldsymbol{r}'\exp(-ik_{\text{scattered}}\boldsymbol{r}'\cdot\boldsymbol{s})\sum_j\frac{1}{\epsilon_0}\delta\epsilon_{xy,j}\,f_j(\boldsymbol{r}')\times\exp(ik_{\text{incident}}z') \quad (12)$$

The depolarized scattering intensity, I, is proportional to the statistical expectation value $\langle EE^*\rangle$; thus

$$I(\mathbf{q}) = I_{\text{inc}}{k_0}^4\left(\frac{1}{4\pi r}\right)^2\int_V\mathrm{d}\boldsymbol{r}'\int_V\mathrm{d}\boldsymbol{r}''\times\exp[-i\boldsymbol{q}\cdot(\mathbf{r}'-\mathbf{r}'')]\sum_j\left(\frac{1}{\epsilon_0}\delta\epsilon_{xy,j}\right)^2\langle f_j(\mathbf{r}')f_j(\mathbf{r}'')\rangle \quad (13)$$

where I_{inc} is the intensity of the incident beam, r is the sample-to-detector distance, and the scattering vector **q** is defined as

$$\mathbf{q} = k_{\text{scattered}}\mathbf{s} - k_{\text{incident}}\mathbf{a}_z \quad (14)$$

The summation over the expectation value, $\langle f_j(\mathbf{r}')f_j(\mathbf{r}'')\rangle$, in eq 13, is done in two steps. We first sum over all grains in the ensemble whose direction of **g** lies within a small solid angle $\mathrm{d}\Omega_g$ and then sum over all values of the solid angle. The two-point expectation value, $\langle f_j(\mathbf{r}')f_j(\mathbf{r}'')\rangle$, summed over all grains whose optic axis lies in a small angular interval, $\mathrm{d}\Omega_g$ is the probability, $C(\mathbf{r}'-\mathbf{r}'',\mathbf{g})\,\mathrm{d}\Omega_g/4\pi$, that both points lie in a grain with optic axis, γ, in that angular interval. We can thus rewrite the sum in eq 13 as

$$\sum_j\left(\frac{1}{\epsilon_0}\delta\epsilon_{xy,j}\right)^2\langle f_j(\mathbf{r}')f_j(\mathbf{r}'')\rangle = (2n_o(n_e - n_o))^2\frac{1}{4\pi}\int_0^{2\pi}d\phi_g\int_0^{\pi}\delta\theta_g\times\sin(\theta_g)(\boldsymbol{a}_x\cdot\boldsymbol{g}\boldsymbol{g}\cdot\boldsymbol{a}_x)^2\boldsymbol{C}(\mathbf{r}'-\mathbf{r}'';\boldsymbol{g}) \quad (15)$$

Substituting eq 15 into eq 13 we get

$$I(\mathbf{q}) = I_{\text{inc}}K\int_0^{2\pi}\mathrm{d}\phi_g\int_0^{\pi}\mathrm{d}\theta_g\times\sin(\theta_g)(\boldsymbol{a}_x\cdot\boldsymbol{g}\boldsymbol{g}\cdot\boldsymbol{a}_y)^2\int_V\mathrm{d}\boldsymbol{r}'\int_V\mathrm{d}\boldsymbol{r}''\times\exp[-i\boldsymbol{q}\cdot(\mathbf{r}'-\mathbf{r}'')]\boldsymbol{C}(\mathbf{r}'-\mathbf{r}'';\boldsymbol{g}) \quad (16)$$

where

$$K = \frac{{k_0}^4}{\pi}\left(\frac{1}{4\pi r}\right)^2{n_o}^2(n_e - n_o)^2 \quad (17)$$

Equation 16 is deceptively similar to our previously derived expression[7] for scattering from randomly oriented ellipsoidal grains embedded in a disordered matrix. The effect of the aligned part of the sample is manifested in the definition of the scattering vector **q**. In the limit of low birefringence ($|n_e - n_o| \ll n_o$) and small scattering angles ($\theta \ll \pi/4$), **q** is given by

$$\boldsymbol{q} = \begin{pmatrix} q_x \\ q_y \\ q_z \end{pmatrix} = k_0 n_o \begin{pmatrix} \theta \cos \mu \\ \theta \sin \mu \\ \phi_{\text{aligned}} \dfrac{\Delta n}{n_o} \end{pmatrix} \tag{18}$$

where $\Delta n = n_e - n_o$ and θ and μ are the polar and azimuthal angles of a laboratory spherical polar coordinate system (see Figure 2).

We see that the scattering vector, **q**, has a nonzero z component even in the paraxial approximation, due to the macroscopic birefringence of the sample (see eq 18). In contrast, for isotropic samples, the scattering vector is restricted to the xy plane in the paraxial approximation. It is convenient to decompose the scattering vector into a transverse component ($\mathbf{q}_T$) and a longitudinal component ($\mathbf{q}_L$):

$$\mathbf{q} = \mathbf{q}_T + q_L \mathbf{a}_Z \tag{19}$$

where

$$q_T = n_o k_0 \theta \quad \text{and} \quad q_L = k_0 \phi_{\text{aligned}} \frac{\Delta n}{n_o} \tag{20}$$

Equations 16 through 20 are the main results of this section, and they apply specifically to the sample shown schematically in Figure 2. Minor differences in sample configuration can be taken into account by redefining the scattering vector. If the polarizer axis is parallel to the optic axis of the aligned grains, then the sign of q_L in eq 20 is reversed. If the sample in Figure 2 is tilted in the xz plane such that $\mathbf{k}_{inc}$ makes an angle ψ with the optic axis of the aligned grains, then Δn in eq 20 is reduced by a $\sin^2\psi$ factor.[36] If the disordered and/or aligned regions are sequestered adjacent to the shear plates, then the incident and scattered wave vectors must be redefined using the appropriate average refractive indices.

Application of Theory

1. Ideal Grains. The simplest situation arises if the sample is composed of individual, randomly shaped grains with (1) a constant optic axis within each grain, (2) no correlation between grain shape and optic axis, and (3) no correlation between optic axes of different grains. We use the term "ideal grains" to characterize such a system. The correlation function of ideal grains, $C(\mathbf{r}' - \mathbf{r}'', \mathbf{g})$, is one that depends only on $\mathbf{R} = \mathbf{r}' - \mathbf{r}''$ and is independent of **g**. Inserting a simple Gaussian correlation function, $C(\mathbf{R},\mathbf{g}) = \exp[-R^2/(2w^2)]$ into eq 16 gives

$$I(\boldsymbol{q}) = I(q) = I_{inc} K V_s \pi^{3/2} w^3 \phi_{\text{grains}} \exp(-w^2 q_T{}^2/2) \exp(-w^2 q_L{}^2/2) \tag{21}$$

In eq 21, the characteristic grain size is given by w and V_s is the scattering volume.

If the same ensemble of grains were embedded in an isotropic matrix, then $I(q)$ is obtained from eq 21 by setting $q_L = 0$. The effect of the birefringent medium is thus to reduce the scattering intensity by a θ-independent factor, $\exp(-w^2 q_L{}^2/2)$. This reduction in intensity is caused by destructive interference between scattered light components generated at different longitudinal locations inside the sample. Consider forward-scattered components generated at two different z locations, z_1 and z_2 ($\Delta z = z_2 - z_1$). Before the scattering event, the incident beam propagates subject to n_o. After scattering, the scattered components propagate subject to n_e. The resulting phase difference between the two scattered beams is thus $2\pi\Delta n \Delta z/\lambda$. Because the scattered intensity is an incoherent sum of contributions from different grains, the phase shift accumulates only over the length scale of one grain, i.e., $\Delta z \approx w$, implying a phase shift of $2\pi\Delta n w/\lambda$. This phase shift is precisely responsible for the intensity reduction described in eq 21.

2. Ellipsoidal Grains. We now consider a random collection of ellipsoidal grains wherein the characteristic size of the grains along the optic axis (**g**) is different from the characteristic size of the grains in the other orthogonal directions (**a** and **b**); **a**, **b**, and **g** are unit vectors. The correlation function of such a sample can be expressed as

$$C(\mathbf{R},\mathbf{g}) = \exp\left(-\left(\frac{\mathbf{a}\cdot\mathbf{R}}{2w}\right)^2\right)\exp\left(-\left(\frac{\mathbf{b}\cdot\mathbf{R}}{2w}\right)^2\right)\exp\left(-\left(\frac{\mathbf{g}\cdot\mathbf{R}}{2l}\right)^2\right) \tag{22}$$

where the characteristic lengths[37] of the ellipsoidal grains in the directions parallel and perpendicular to the optic axes are l and w, respectively.

Substituting eq 22 into eq 16 gives the following expression for the scattered intensity

$$I(\mathbf{q}) = I_0[C(\mathbf{q}) + D(\mathbf{q}) \cos 4\mu] \tag{23a}$$

where

$$I_0 = I_{inc} K V_s \pi^{3/2} w^2 l \phi_{\text{grains}} = K_c w^2 l \phi_{\text{grains}} \tag{23b}$$

The explicit expressions for the functions $C(\mathbf{q})$ and $D(\mathbf{q})$ are given in the appendix. We find that $C(\mathbf{q})$ and $D(\mathbf{q})$ are only functions of the magnitudes of **q**: q_T and q_L. This implies that the scattering profiles predicted by eq 23 exhibit 4-fold symmetry. The 4-fold symmetry we get in eq 23 is consistent with a uniform angular distribution of the optic axes of the unaligned grains. If, however, the unaligned grains in the sample were characterized by a nonuniform angular distribution then the 4-fold symmetry of the scattering pattern could be broken.

3. **Neglecting Birefringent Background.** It is evident from eq 21 that the effect of the birefringent medium on scattering from ideal grains is negligible if $q_L w = 2\pi|\Delta n| w/\lambda \ll 1$. For ellipsoidal grains, it is evident from eqs A1 and A2 that the effect of the birefringent medium on scattering from the grains is negligible when both $q_L w$ and $q_L l$ are much smaller than unity. As stated in the Introduction, grain dimensions for a wide variety of polymeric systems range from 1 to 10 μm. This implies that w/λ (or equivalently l/λ) ranges from 2 to 20 (assuming $\lambda = 0.5$ μm). In most other crystalline and liquid crystalline materials, $|\Delta n|$ is on the order of 10^{-1}; thus, $q_L w$ ranges from 1 to 10, and the birefringent medium has a substantial effect on scattering from the coexisting grains. For the case of polystyrene−polyisoprene block copolymers, however, $|\Delta n|$ is on the order of 10^{-4}, $q_L w$ ranges from 10^{-3} to 10^{-2}, and to a very good approximation, $\mathbf{q} = \mathbf{q}_T$. In this case, the scattering profiles are identical to those that would be obtained from the ellipsoidal grains if they were embedded in an isotropic matrix. In the theory section, it was assumed that the refractive index of the medium between the sample and the detector had a refractive index n_o. In our experiments, the medium between the sample and

the detector is air, and this can be taken into account by defining $|\mathbf{q}| = |\mathbf{q}_T| = 4\pi(\sin(\theta/2)/\lambda)$. The depolarized scattered intensity profile, $I(\mathbf{q})$, from such a sample is given by eq 23. The functions $C(q)$ and $D(q)$, obtained by setting $q_L = 0$ in eqs A1 and A2, are identical to those given in ref 7

$$C(q) = \exp\left[-\frac{q^2w^2}{2}\right]\int_0^{\pi} d\alpha \sin^5\alpha \exp[-\beta(\alpha)]I_0[\beta(\alpha)] \quad (24)$$

and

$$D(q) = \exp\left[-\frac{q^2w^2}{2}\right]\int_0^{\pi} d\alpha \sin^5\alpha \exp[-\beta(\alpha)]I_2[\beta(\alpha)] \quad (25)$$

where $\beta(\alpha) = (q^2l^2/4)[1 - w^2/l^2] \sin^2\alpha$, and I_m is the modified Bessel function of order m.

The ratio of the total scattered power, P, to the incident power, P_0, was obtained by integrating eq 23 over all values of θ and μ

$$\frac{P}{P_0} = \frac{4\pi^2}{15}(\Delta n)^2\frac{L\phi_{grains}l_{av}}{\lambda^2} \quad (26)$$

where L is the sample thickness in the z direction and l_{av}, the characteristic dimension of the grains, is given by

$$l_{av} = \frac{15}{16}\sqrt{2\pi}\, wf(a) \quad (27)$$

In eq 27, $a = [1 - (w/l)^2]^{1/2}$, and the function $f(a)$ is given by

$$f(a) = \frac{1}{4a^2}\left[\sqrt{1-a^2}(6a^2 - 3) + (3 - 8a^2 + 8a^4)\frac{\arcsin(a)}{a}\right] \quad (28)$$

The principal value of the arcsin function should be used in the evaluation of eq 28. In the special case that $l = w$, then $a = 0$, $f(0) = 16/15$, and $l_{av} = \sqrt{2\pi}\, w$. This corresponds to previously published results for P/P_0.[36,38,39]

Finally, we give the equations that we use to analyze the birefringence experiments wherein the sheared sample is rotated so that the polarizer and analyzer are at ±45° to the optic axis of the single crystal. Neglecting scattering contributions in this instrument configuration is justified in the single scattering limit. Under these conditions, the ratio of the transmitted power to the incident power is given by[34]

$$\frac{P}{P_0} = \sin^2(\Gamma\phi_{aligned}/2); \qquad (\phi_{aligned} \neq 0) \quad (29)$$

where Γ is the retardation of a perfect single-crystal sample with path length L, $\Gamma = 2\pi L\Delta n/\lambda$. Equation 29 applies when $0 < \Gamma\phi_{aligned} \leq \pi$. For larger retardation, e.g. $\pi \leq \Gamma\phi_{aligned} \leq 2\pi$

$$\frac{P}{P_0} = \sin^2(\pi - \Gamma\phi_{aligned}/2); \qquad (\phi_{aligned} \neq 0) \quad (30)$$

Equations 23−30 are the main results of our theoretical analysis. For partially aligned block copolymer samples shown in Figure 2, the detection of birefringence is related to the aligned crystal (eqs 29 and 30), while the depolarized light-scattering signal is related to the randomly oriented grains (eq 23). We demonstrate that appropriate experiments can give quantitative estimates of both ϕ_{grains} and $\phi_{aligned}$. The depolarized light-scattering intensity from a perfect single crystal ($\phi_{grains} = 0$ and $\phi_{aligned} = 1$) is zero (see eq 23). However, the birefringence signal from a sample completely filled with randomly oriented grains ($\phi_{grains} = 1$ and $\phi_{aligned} = 0$) is not zero. It is proportional to the average grain size as indicated by eq 26. Equations 29 and 30 apply only when a significant fraction of the sample is aligned so that P/P_0 is much larger than that obtained from randomly oriented grains.

Experimental Description

A polystyrene−polyisoprene diblock copolymer was synthesized by anionic polymerization under high vacuum, using methods described elsewhere.[40] The weight-average molecular weights of the polystyrene and polyisoprene blocks are 6.5 and 18.4 kg/mol, respectively, and we refer to this polymer as SI(7−18). The polydispersity index is 1.07. The polymer characterization procedures are given in ref 40. About 0.5 wt % BHT (2,6-di-*tert*-butyl1−4-methylphenol) was added to a benzene solution of the polymer to prevent oxidative degradation. The polymer was isolated by freeze-drying and stored in a freezer at −11 °C.

DSC scans at a heating rate of 10 °C/min were conducted on a fully ordered SI(7−18) melt. These measurements indicated that the glass transition temperature of the polystyrene microphase was 54 °C.[19] The order−disorder transition temperature, T_{ODT}, of SI(7−18) was determined by the local birefringence method[41,42] and found to be 105 ± 1 °C. The volume fraction of polystyrene in the block copolymer is 0.23. On the basis of extensive characterization of polystyrene−polyisoprene block copolymers, we expect the sample to have a cylindrical microstructure at temperatures below 105 °C.[43] The scattering experiments under shear flow were conducted at 85 °C.

Figure 3 is a schematic of the instrument that was used to study the optical properties of the block copolymer melt under shear flow.[44] It consists of three parts: a computer-controlled shear device, optical trains for both birefringence and SALS measurements, and a data acquisition system supported by LabView software.

The shear cell, shown in Figure 3a, consists of two aluminum parallel plates fitted with quartz windows (1.5 in. diameter, 0.5 in. thick disks) to allow for the passage of light. The plate was mounted on a linear positioning table that was driven by a microstepping motor. The time dependence of the displacement of the top plate was approximately triangular. The strain amplitude was held fixed at 133% during all of the shear flow experiments. The shear plate velocity was controlled (at 0.1 and 1 mm/s for the usual sample thickness of 1.5 mm) to obtain shear rates, $\dot{\gamma}$, of 0.067 and 0.67 s^{-1}. The temperature of the bottom plate, which served as the heating block, was controlled by electrical heating rods and a thermocouple embedded in the heating block. The relationship between the set temperature and the sample temperature was determined in separate experiments by inserting a thermocouple into the sample.

The same shear cell (Figure 3a) was used to perform two kinds of measurements: (1) depolarized light-scattering measurements, described in Figure 3b, and (2) birefringence measurements, described in Figure 3c. A He−Ne laser with wavelength $\lambda = 0.633$ μm was used as the light source. The beam was directed through a halfwave plate and a polarizer before it reached the sample. Neutral density filters (not shown in Figure 3 for simplicity) were used to adjust the intensity of the incident beam so that the detected signal was within the dynamic range of the detector. The halfwave plate was used

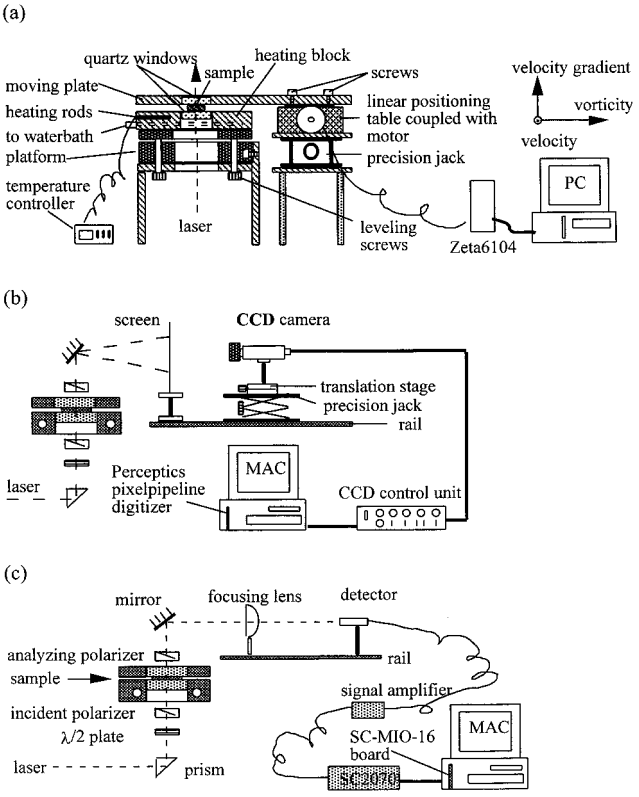

Figure 3. Schematic view of the (a) shear cell, and optical trains for (b) depolarized light-scattering experiments and (c) birefringence under shear flow.

to change the polarization direction of the incident beam. In both experiments, the light emerging from the sample passed through an analyzing polarizer and reflected off a mirror. The polarizer and analyzer axes were always orthogonal to each other.

Depolarized Light Scattering under Shear Flow. Figure 3b shows a schematic of the depolarized light-scattering instrument. The detection system consists of a paper screen held between optical flats and an MTI Dage CCD72 camera equipped with a Sigma super-wide-II lens. The distance between screen and camera was kept at 18 cm during all of the measurements. The distance between sample and mirror was always 82 mm, and the distance from mirror to screen was adjustable depending on the size of scattering pattern on the screen. A scattering pattern with a size of 1−1.5 in. in diameter was chosen as ideal for image capture, and was obtained by moving the screen and camera. The signals from the camera were digitized and recorded by the computer. The light-scattering experiments involved measuring the time dependence of the scattering profile, $I(\theta,\mu)$, under both quiescent and flow conditions (see Figure 3).

The time dependence of the scattering intensity, I, along directions of $\mu = 0°$ and 45° (see Figure 2) was measured as a function of scattering vector $q = (4\pi/\lambda)\sin(\theta/2)$. The procedures used to acquire these data were identical to those described in ref 7 for depolarized light-scattering measurements on quiescent samples. It took about 80 s for the camera to acquire data along both $\mu = 0$ and 45° directions. At $\dot{\gamma} = 0.067\ s^{-1}$, the sample had received two reciprocating strokes per exposure, while at $\dot{\gamma} = 0.67\ s^{-1}$, the sample had received 20 reciprocating strokes per exposure. Under shear flow, the depolarized light-scattering measurements were performed with the shear direction parallel to the analyzer axis. In the absence of shear flow, the depolarized scattering data were independent of direction of the polarizer/analyzer axes. In most experiments a central bright spot was observed and this prevented obtaining scattering data in the range $0 \le q \le 0.2\ \mu m^{-1}$. The scattered intensity obtained in the disordered state was treated as background and subtracted from the measured signal. We only used scattering data when they were a factor of 2 above the background.

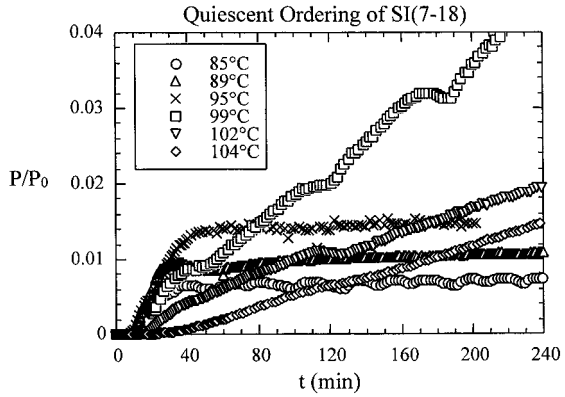

Figure 4. Time dependence of the birefringence signal (P/P_0) from quiescently ordered SI(7−18) at the selected temperatures, after quenching from the disordered state.

Birefringence Measurements. Birefringence of the sample under shear flow was measured using the setup shown in Figure 3c. Under shear flow, measurements were made with the incident beam polarization at an angle of at 45° relative to the flow direction. In the absence of shear flow, the measured signal was independent of direction of the polarizer/analyzer axes. The light reflected from the mirror was focused onto a photodiode. The distance from sample to mirror to focusing lens was 165 mm, and the diameter and focal length of the lens were 51 and 70 mm, respectively. The photodiode signal was digitized and recorded using LabView. The signal was converted to P/P_0, where P is the power at the detector and P_0, the incident power, was obtained by rotating the analyzer so that its axis was parallel to that of the polarizer and inserting the appropriate neutral density filters.

Samples were prepared by placing approximately 1 g of block copolymer on the bottom quartz window. A retaining Teflon ring (19 mm inner diameter and 2 mm thickness) was placed around the sample, and this assembly was placed in a vacuum oven at 120 °C for 12 h. Under these conditions the polymer melted, and a bubble-free, disk-shaped sample was obtained. The retaining ring was removed and the quartz window was attached to the bottom plate. The top plate and motor assembly were then lowered until a flat sample with 1.5 mm thickness and 25 mm diameter was obtained. The incident light beam had a waist diameter of about 1 mm, and it was located at the center of the sample. The large sample diameter ensured that edge effects were negligible.

Each experiment was started by disordering the sample at 110 °C (a temperature of a few degrees above the T_{ODT}) for 60 min to erase the effect of thermal and shear history. Samples were then quenched to a predetermined temperature below T_{ODT}. In both the quiescent and shear experiments, time zero ($t = 0$) was defined as the time when the temperature set point on the controller was changed. The shear field was applied at $t = 0$, when the sample was in the disordered state. The sample temperature reached within 1 °C of the final target temperature in about 10 min. Each experiment reported here was repeated several times to ensure reproducibility which was within 10%; for clarity and brevity, we only show 1 data set.

Results and Discussion

Quiescent Grain Structure. We begin by studying ordering kinetics of SI(7−18) under quiescent conditions. The sample was first disordered by heating to 110 °C, as usual, and then quenched to several temperatures below T_{ODT}. The time dependence of the birefringence signal, P/P_0, after quenching, recorded using the apparatus shown in Figure 3c with the motor turned off, is shown in Figure 4. We use eq 26 to interpret the data in Figure 4. It is evident from eq 26 that P/P_0 changes

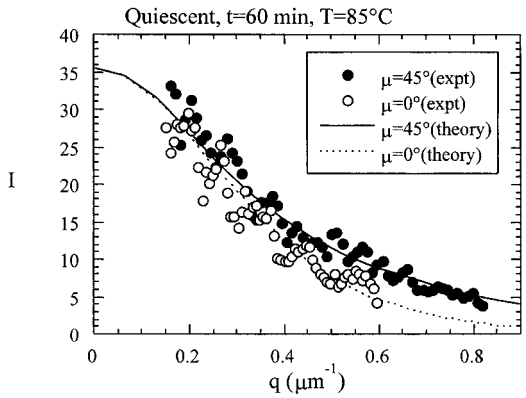

Figure 5. Quiescent depolarized light-scattering data along $\mu = 0$ and 45° directions at $t = 60$ min. The curves are the theoretical fits (eqs 23−25) with l, w, and I_0 as adjustable parameters.

during ordering due to changes in both l_{av} (the characteristic grain dimension) and ϕ_{grains} (the volume fraction of ordered grains). During the early stages of ordering, both l_{av} and ϕ_{grains} increase with time as randomly oriented grains grow at the expense of the disordered phase.[7,45] When P/P_0 reaches a stable value, it implies that both l_{av} and ϕ_{grains} do not change with time. In previous work[7,45,46] we have shown that this is a signature that ϕ_{grains} has reached its asymptotic value of unity. Thus, the time required for P/P_0 to reach a stable value provides an estimate of the time required to complete the disorder to order transition. At the large quench depths ($T \leq 95$ °C) the disorder to order transition is completed in 45 min or less (see Figure 4). The fact that l_{av} becomes time independent implies that the grain structure is stable, i.e., the intervening defects are not mobile on the time scale of the experiments. At small quench depths ($T \geq 99$ °C) the time dependence of P/P_0 is quite different from that at large quench depths ($T \leq 95$ °C). We find that P/P_0 increases continuously even at $t = 240$ min; see Figure 4. A possible reason for this is that the ordering kinetics at these small quench depths is slow, and it takes more than 240 min for ϕ_{grains} to reach its asymptotic value of unity. A more likely explanation is that $\phi_{grains} = 1$ at $t < 240$ but P/P_0 increases because of the annihilation of defects between grains, which leads to increasing l_{av}. In previous experiments on another polystyrene−polyisoprene block copolymer[7] we had found similar behavior at small quench depths (i.e., high temperature). It is evident that the ordering kinetics of SI(7−18) at $T \geq 99$ °C is quite complex even under quiescent conditions. Since the focus of this study is the effect of shear flow on ordering, we conducted our shear-ordering experiments at a large quench depth, wherein the quiescent behavior is simple, and the ordering transition is completed in a reasonable amount of time. In the remainder of this paper, we focus on order formation after quenching the sample from the disordered state to 85 °C.

Depolarized light-scattering profiles after quenching SI(7−18) from the disordered state to 85 °C were measured as a function of time using the apparatus shown in Figure 3b with the motor turned off. Typical data are shown in Figure 5 where we show $I(q)$ along $\mu = 0$ and 45° at 60 min. These data are qualitatively similar to those reported in ref 7 and consistent with the single ellipsoidal grain model. The curves in Figure 5 are the results of theoretical calculations, using eq 23a, with grain dimensions (l and w) and I_0 as adjustable parameters. The theoretical scattering profiles for a chosen pair of l and w values were computed by first numerically integrating the integrals in eqs 24 and 25 to obtain $C(q)$ and $D(q)$, and then substituting these functions into eq 23a to enable the computation of $I(q,\mu)$. From eq 23a, it is evident that $I(q,\mu=0°) = I_0[C(q) + D(q)]$ while $I(q,\mu=45°) = I_0[C(q) - D(q)]$. The value of I_0 was then adjusted to obtain the best least squares match between theory and experiment along both $\mu = 0$ and 45° directions, and the sum of the squares of the difference between theory and experiment was noted. The procedure was repeated for a range of l and w values. The combination of I_0, l, and w that minimized the sum of the squares of the difference between theory and experiment was used to draw conclusions about the grain structure. As reported in previous studies,[7,46] our fits typically give standard deviations of ±5% for l and w and ±10% for I_0. It is evident in Figure 5 that our theory captures the essential features of the experimental data. Electron microscopy has shown the complex and polydisperse shape of grains obtained in a quiescently ordered block copolymer.[39] The fact that the statistical properties of the grains can be described by a two-parameter correlation function is a significant simplification. From the fitting procedure, we conclude that at $t = 60$ min, the characteristic grain volume, $v \equiv lw^2$ is 14 μm^3, and the characteristic grain dimension, l_{av} is 4.2 μm (from eqs 27 and 28). At times, $t \geq 60$ min, the scattering signal was time-independent, indicating that the sample is fully occupied by randomly oriented, stable grains. The proportionality constant K_c in eq 23b was determined, using the value $\phi_{grains} = 1$ at this point, and known values of lw^2 and I_0. This enables the evaluation of the time dependence of the grain structure at $T = 85$ °C from the time-dependent depolarized light-scattering profiles. The time dependence of v and ϕ_{grains} thus determined is given in Table 1. The ordering process is completed in 20 min ($\phi_{grains} = 1$ at this time). However, the grain volume (v) continues to increase slowly at times $20 < t < 60$ due to defect annihilation. The defect annihilation processes cease to be effective at times greater than 60 min, and a frozen grain structure is obtained.

Table 1. Microstructure Development of SI(7−18) under Quiescent Conditions at 85 °C

t (min)	w (μm)	l (μm)	l/w	v (μm)^3	ϕ_{grains}
10[a]					
17	1.34	5.36	4.0	9.62	0.90
20	1.40	5.60	4.0	11.0	1.01
30	1.43	5.72	4.0	11.7	1.04
60	1.51	6.04	4.0	13.8	1.00

[a] Grain parameters could not be determined at $t \leq 10$ min due to lack of signal.

The 85 °C data in Figure 4 show that P/P_0 reaches a plateau of about 0.007 at long times. We can use eq 26 to estimate Δn because all other quantities in eq 26 are known (note that l_{av} was determined in the preceding paragraph and $\phi_{grains} = 1$). We find that $\Delta n = 4.1 \times 10^{-4}$. We can also estimate Δn for a medium consisting of cylinders embedded in a matrix.[34] Using the composition of the block copolymer, the volume fractions of the polystyrene and polyisoprene blocks are $f_{PS} = 0.233$, $f_{PI} = 0.767$, respectively, and the refractive indices of these materials are $n_{PS} = 1.59$, and $n_{PI} = 1.52$. Using well-established expressions,[34] Δn is calculated to be 5.7×10^{-4}. This value corresponds to the Δn of SI(7−18) due

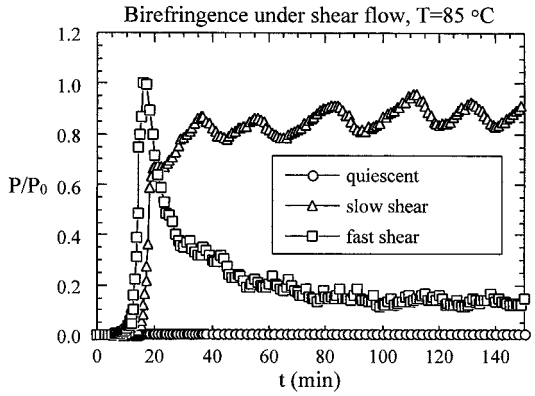

Figure 6. Time dependence of the birefringence signal (P/P_0) from SI(7−18) under shear flow after quenching from the disordered state to T = 85 °C. Data obtained under quiescent conditions are also shown for reference.

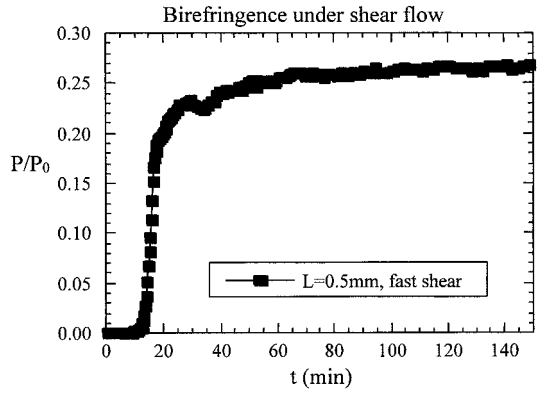

Figure 7. Time dependence of the birefringence data signal (P/P_0) from a 0.5 mm thick SI(7−18) sample under fast shear flow ($\dot{\gamma}$ = 0.67 s^{-1}) after quenching from the disordered state to T = 85 °C.

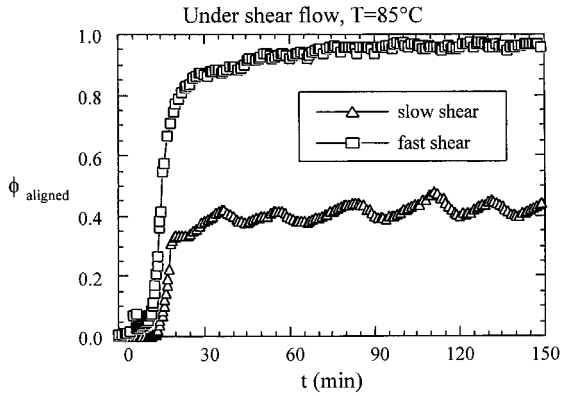

Figure 8. Time dependence of $\phi_{aligned}$, the single-crystal volume fraction under shear flow at T = 85 °C for slow ($\dot{\gamma}$ = 0.067 s^{-1}) and fast ($\dot{\gamma}$ = 0.67 s^{-1}) shear flow.

to form birefringence, in strong segregation limit. Intrinsic birefringence contributions are expected to increase Δn by about 30%.[47] We estimate $\Delta n = 7.4 \times 10^{-4}$ in the strong segregation limit. As expected, Δn for SI(7−18) at 85 °C is lower than that in the strong segregation limit. This is undoubtedly due to the proximity of the sample to the order−disorder transition temperature. We are not aware of explicit estimates of Δn for cylindrical block copolymers in the weak segregation limit.

Structure under Shear Flow. The time dependence of P/P_0 obtained under shear flow is shown in Figure 6. For comparison, we also show data, obtained under quiescent conditions, in the same figure. The magnitude of P/P_0 under flow is about 2 orders of magnitude larger than that under quiescent conditions, due to alignment of the cylinders. All of the previous studies on shear alignment of block copolymer cylinders [e.g., refs 23−25 and 27] have shown that the cylinder axes are aligned parallel to the flow direction. We have thus assumed that the cylinder axes in SI(7−18) also align in the flow direction (Figure 2). We note, however, that the birefringence signal, obtained in the unlikely event that the cylinders in our sample were aligned perpendicular to the flow direction, would be identical to that reported here. Under slow shear conditions ($\dot{\gamma}$ = 0.067 s^{-1}), P/P_0 reaches a steady value of about 0.9 in 40 min. In contrast, the signal under fast shear ($\dot{\gamma}$ = 0.67 s^{-1}) increases rapidly until t = 16 min then decreases. One possibility is that shear-induced disordering occurs under these conditions. Another possibility is that the retardation of the sample has exceeded a half wave ($\Gamma\phi_{aligned} > \pi$). The cusplike shape of the $P(t)/P_0$ curve and the fact that the decrease began when P/P_0 was in the vicinity of unity suggest that the latter is the case.

To decide between these two possibilities, we conducted birefringence measurements under fast shear with reduced sample thickness (from 1.5 to 0.5 mm). The velocity of the shear plate and the amplitude of the motion were correspondingly reduced to maintain the same shear rate (0.67 s^{-1}) and shear amplitude (133%). The birefringence data from the sample with L = 0.5 mm ($\dot{\gamma}$ = 0.67 s^{-1}) are shown in Figure 7. It is evident that, in this case, P/P_0 reaches a plateau after 60 min. If the imposition of $\dot{\gamma}$ = 0.67 s^{-1} had caused disorder then the P/P_0 signal in Figure 7 would decrease after 16 min as it did with the L = 1.5 mm sample (Figure 6, fast shear). We therefore conclude that the decrease in signal seen at $\dot{\gamma}$ = 0.67 s^{-1} in Figure 6 is due to $\pi <$ $\Gamma\phi_{aligned} < 2\pi$. To convert the $P(t)/P_0$ data in Figure 6 into single-crystal volume fraction, $\phi_{aligned}(t)$, for $\dot{\gamma}$ = 0.67 s^{-1}, we use eq 29 for $t \leq$ 16 min and eq 30 for $t >$ 16 min, while for $\dot{\gamma}$ = 0.067 s^{-1} we use eq 29 at all times. The results are shown in Figure 8 where we plot the time dependence of $\phi_{aligned}$ under slow and fast shear flow. Under fast shear, the single-crystal volume fraction approaches unity at long times. Under slow shear, about 40% of the sample is converted to a single crystal. It is evident that for SI(7−18) at 85 °C a shear rate of $\dot{\gamma}$ = 0.67 s^{-1} is more effective in producing alignment than $\dot{\gamma}$ = 0.067 s^{-1}.

Our conclusions regarding the time dependence of $\phi_{aligned}$ are based on the assumption that the block copolymer morphology under shear flow depends only on imposed shear rate and shear amplitude and is independent of sample thickness. While we expect this to be qualitatively true, we are not aware of any published data indicating that this is a quantitative fact. In fact, a number of researchers (including our group) have presented data indicating that the block copolymer microstructure close to the container walls is significantly distorted.[21,48] A quantitative comparison of the data obtained at L = 0.5 and 1.5 mm under fast shear indicate that microstructures formed in these two experiments are not identical. In particular, the retardation of the 0.5 mm sample is about half of that expected from measurement on the 1.5 mm sample. In other words, we have significantly increased disorder when the sample thickness is decreased from 1.5 to 0.5 mm. This is not entirely surprising. Jager-Lezer et

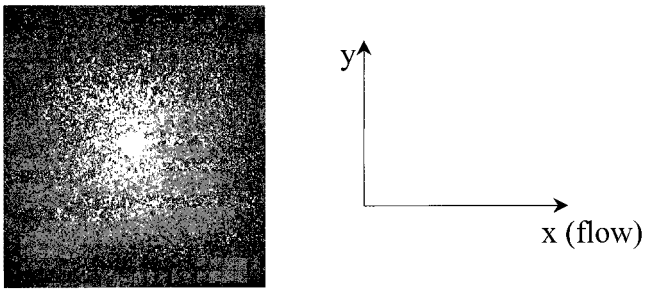

Figure 9. Two-dimensional light-scattering profiles obtained under shear flow at $\dot{\gamma} = 0.067\ s^{-1}$, $t = 50$ min, and $T = 85$ °C. The bright central spot represents the incident beam.

al. have found that the structure of lamellar phases formed by small molecule amphiphiles under shear flow depends on gap size and the chemical constitution of the shear plates.[49] In future work, we will use a combination of electron microscopy and in situ optical experiments to probe details regarding the effect of gap size on block copolymer morphology under shear flow. Because of the above-mentioned uncertainties, all of the remaining experiments were conducted on a 1.5 mm sample under shear flow.

Our birefringence experiments led to the conclusion that most of the sample was converted to a single crystal under fast shear while under slow shear only 40% of the sample was converted to a single crystal. The experiments described thus far do not shed any light on the state of the remaining 60% of the sample under slow shear. We thus address the possibility of obtaining unaligned grains under shear flow by conducting in situ depolarized light-scattering experiments using the apparatus described in Figure 3b. The SI(7−18) sample was subjected to the same thermal and shear history as that used to obtain the data shown in Figure 8. During first 10 min of shearing of both slow shear and fast shear experiments, the measured scattering profiles under shear were indistinguishable from the scattering signal in the disordered state. Recall that we start shearing the sample right after the quench from the disordered state is initiated and that 10 min is comparable to the time required for the sample temperature to reach its final value. Our instrument is incapable of resolving morphological changes at $t \leq 10$ min. A typical image captured by the CCD camera at later times during shear flow is shown in Figure 9. To a good approximation, the profile exhibits 4-fold symmetry, indicating the presence of randomly oriented ellipsoidal grains. We note, in passing, that this is not a general property of block copolymers under flow. Scattering profiles from other polystyrene−polyisoprene block copolymers that we have studied showed substantial deviations from 4-fold symmetry. Analysis of the grain structure in such samples will be discussed in future publications.

Typical depolarized light-scattering profiles obtained from the slow shear experiment are shown in Figure 10. In Figure 10a we show data obtained at $t = 17$ min while in Figure 10b we show data obtained at $t = 60$ min. The scattering intensity increases with time indicating the increasing presence of randomly oriented grains under shear flow. The magnitude and q dependence of scattering intensity is comparable to that obtained under quiescent conditions; compare Figures 5 (quiescent data at $t = 60$ min) and 10b (slow shear data at $t = 60$ min). Thus, the qualitative nature of the

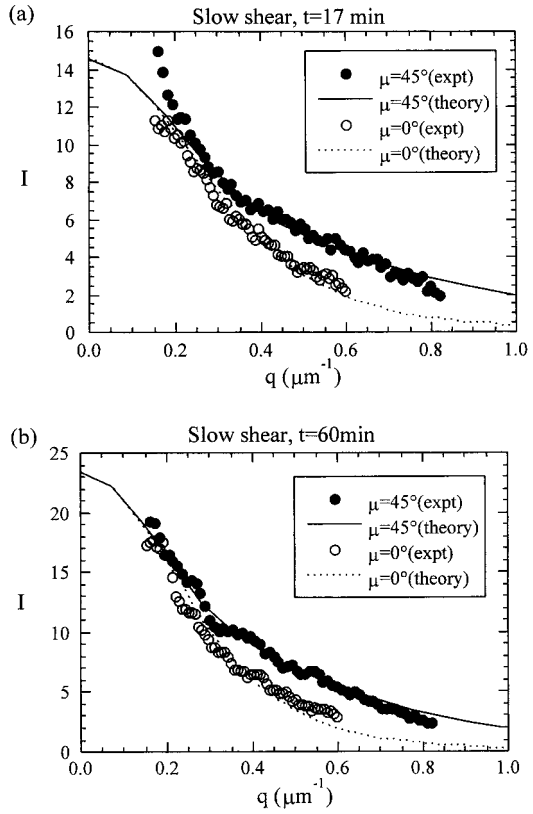

Figure 10. Depolarized light-scattering profiles at (a) $t = 17$ min and (b) $t = 60$ min under slow shear flow ($\dot{\gamma} = 0.067\ s^{-1}$). The curves are the theoretical fits (eqs 23−25) with l, w, and I_0 as adjustable parameters.

randomly oriented grains formed under shear flow is similar to that of grains formed under quiescent conditions. The light-scattering data under shear flow (e.g., Figure 10) were analyzed using eq 23 with the same procedure as that used to analyze the quiescent scattering data. Rigorous justification for the use of these equations is given in the Theoretical Analysis section. The curves in Figure 10 represent least-squares fits through the $\mu = 0$ and 45 ° data, from which we obtain the time dependence of I_0, l, and w. The value of I_0 can be converted to ϕ_{grains} using eq 23b because K_c, w, and l are known. Recall that the constant, K_c, was determined from the quiescent light-scattering and birefringence data. The data obtained under fast shear were subjected to a similar analysis. In Figure 11 we show the scattering profiles obtained under fast shear flow ($\dot{\gamma} = 0.67\ s^{-1}$) at $t = 17$ and 30 min. The scattered intensity is significantly lower than that under slow shear; compare Figures 11 and 10. This implies that the concentration of randomly oriented grains that are present under fast shear are significantly lower than that obtained under slow shear. The curves in Figure 11 represent least-squares theoretical fits which we use to characterize the randomly oriented grains that grow and survive under fast shear.

In our model, the ordered structure under shear flow is characterized by four independent parameters: l, w, and ϕ_{grains}, which characterize the random grain structure, and $\phi_{aligned}$, which characterizes the single crystal. If the sample contains some disordered regions, then $\phi_{grains} + \phi_{aligned}$ will be less than unity. On the other hand, if the disorder to order transition under shear flow is completed, then $\phi_{grains} + \phi_{aligned}$ must equal unity (within experimental error). The birefringence experi-

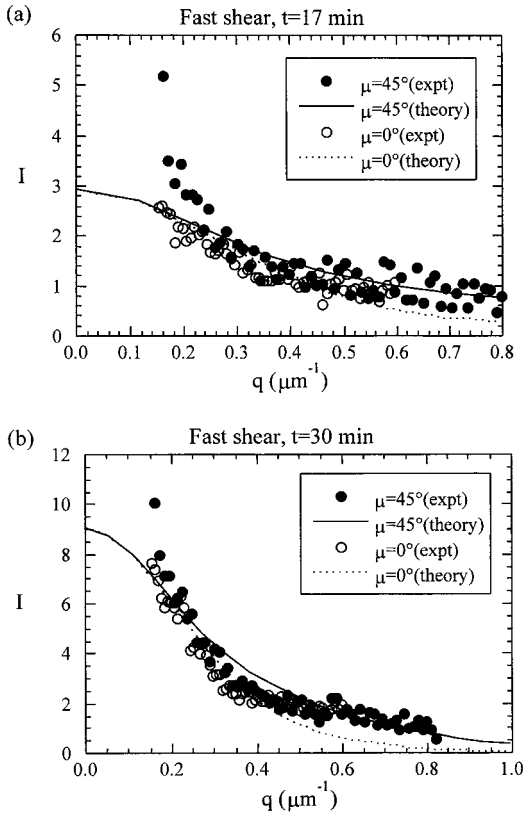

Figure 11. Depolarized light-scattering profiles under shear flow at (a) $t = 17$ min and (b) $t = 30$ min under fast shear ($\dot{\gamma} = 0.67$ s^{-1}). The curves are the theoretical fits (eqs 23−25) with l, w, and I_0 as adjustable parameters.

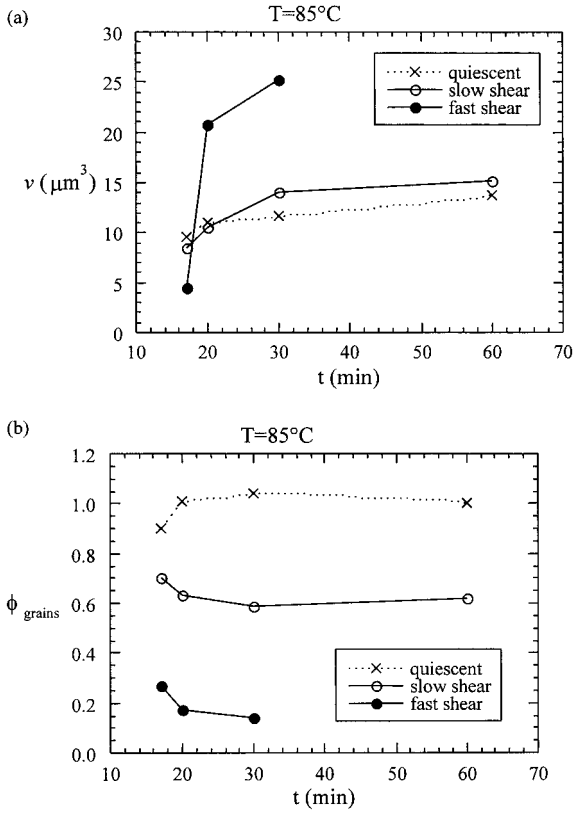

Figure 12. Time dependence of (a) grain volume, v, and (b) volume fraction of randomly oriented grains, ϕ_{grains} under shear flow and under quiescent conditions.

ments gave us the time dependence of $\phi_{aligned}$ under slow and fast shear at 85 °C (Figure 8). The depolarized light-scattering measurements gave us l, w, and ϕ_{grains}. We have thus completely analyzed the grain structure of SI(7−18) under slow and fast shear at 85 °C.

In Figure 12 we compare microstructural evolution under flow with that obtained under quiescent conditions. In Figure 12a we show the time dependence of grain volume, v ($v = w^2 l$), while in Figure 12b, time dependence of the volume fraction of randomly oriented grains, ϕ_{grains}, is shown. The $v(t)$ data obtained under slow shear flow and quiescent conditions are very similar (Figure 12a). The main difference between the quiescent and slow shear experiments can be seen in the $\phi_{grains}(t)$ data shown in Figure 12b. Randomly oriented grains fill the entire sample under quiescent conditions while only 60% of the sample is filled by randomly oriented grains under slow shear. Under fast shear, somewhat larger grains are obtained, but the fraction of the sample filled with randomly oriented grains is only 14% at $t = 30$ min (Figure 12b). At longer times ($t > 30$ min), the scattering data are comparable to background in most directions except for a sharp streak parallel to the flow direction. We do not know the origin of this streak; however, birefringence data (Figure 8) indicate that more than 90% of the sample consists of aligned grains at this point. We thus were unable to study the grain characteristics under fast shear flow when $t > 30$ min, due to lack of signal when ϕ_{grains} falls below 0.1.

Our results for the microstructural evolution of SI(7−18) under shear flow are summarized in Table 2. Under both slow and fast shear, the sum of the volume fractions of random grains and single crystal, $\phi_{aligned} + \phi_{grains}$, sum to unity (within 2%) after $t = 30$ min. This implies that the time scale for completing the disorder to order transition under quiescent conditions (Table 1) and shear flow (Table 2) are similar. The main difference is in the grain structure obtained after completion. Under slow shear flow, the birefringence experiments indicated that only 40% of the sample was converted to a single crystal (Table 2). Independent depolarized light-scattering experiments revealed that the remaining 60% of the sample was in the form of randomly oriented grains. In contrast, birefringence experiments under fast shear flow indicated that most of the sample (97%) was converted to a single crystal. Corresponding depolarized light-scattering signals under fast shear were comparable to the background, indicating the absence of unaligned grains. The consistency between birefringence and depolarized light-scattering experiments under both slow and fast shear provides considerable support for the simple model that we have proposed.

Table 2. Microstructure Development of SI(7−18) under Shear Flow at $T = 85$ °C

$\dot{\gamma}$ (s^{-1})	t (min)	w (μm)	l (μm)	l/w	v (μm^3)	ϕ_{grains}	$\phi_{aligned}$	$\phi_{grains} + \phi_{aligned}$
0.067	17	1.19	5.95	5.0	8.4	0.70	0.20	0.90
	20	1.33	5.99	4.5	10.6	0.63	0.34	0.97
	30	1.46	6.57	4.5	14.0	0.59	0.39	0.98
	60	1.50	6.75	4.5	15.2	0.62	0.40	1.02
0.67	17	0.91	5.43	6.0	4.45	0.27	0.66	0.93
	20	1.73	6.92	4.0	20.7	0.17	0.77	0.94
	30	1.93	6.76	3.5	25.2	0.14	0.87	1.01
	150[a]						0.97	

[a] Grain parameters could not be determined at $t > 30$ min due to lack of signal.

Our model is not able to account for all of our observations such as the streak seen from the almost perfect single crystal under fast shear and the increased low angle scattering in Figures 10 and 11 ($\mu = 45°$, $q < 0.21\ \mu m^{-1}$). Both features indicate the presence of large-scale structures that are not present in our model. An obvious limitation of our model is that we have assumed the existence of a perfect single crystal (see Figure 2). In practice, one expects a mosaic spread in the orientation of the optic axis within the single crystal. Additional parameters are necessary to characterize the length scale over which the optic axis changes direction in the "single crystal". Since there are three independent directions, there may be three length scales associated with the mosaic spread. It is likely that these characteristic lengths are much larger than the size of the randomly oriented grains. Thus, from the rigorous point of view, the sample is composed of (at least) two types of grains: large grains with optic axes centered on the *x* axis, and small grains with randomly oriented optic axes. One may also find large grains with optic axis that are not in the vicinity of the *x* axis, due to effects such as grain rotation or grain wagging under shear flow. Birefringence and depolarized light scattering are not well suited for studying the nature of the mosaic spread and large-scale grain structure in sheared block copolymers. It may be possible to combine the experimental methods developed here with other methods such as in situ optical microscopy for such studies. It is clear that analysis of grain structure using more realistic (and complex) models than that used here will require input from additional experiments.

Concluding Remarks

A combination of in situ birefringence and depolarized light-scattering experiments was used to provide a complete description of the formation of shear-induced microstructure in a block copolymer melt. The birefringence experiments track the formation of the aligned single crystal while the depolarized light-scattering experiments track the formation of randomly oriented grains. We developed an expression for depolarized light scattering from randomly oriented, uncorrelated, grains embedded in the single crystal. Our treatment is perfectly general and applies to any uniaxial sample. We demonstrated that the scattering from such systems could be predicted by the usual scattering formula provided one recognizes that the scattering vector, $\mathbf{q}$, has both transverse and longitudinal components ($\mathbf{q}_T$ and $\mathbf{q}_L$, respectively). A convenient feature of the SI-(7−18) block copolymer used in this study is that $w|\mathbf{q}_L| \ll 1$. This implies that to a very good approximation, $\mathbf{q} = \mathbf{q}_T$, although the total retardation of the sample, $\Gamma\phi_{aligned}$, is substantial.

An instrument that enables both birefringence and depolarized light-scattering experiments was built and used to follow the development of ordered morphology in a melt of SI(7−18) block copolymer under shear flow. The sample was thermally quenched from the disordered to the ordered state and the shear flow was applied as soon as the quench was initiated. Upon completion of the ordering process under slow shear flow ($\dot{\gamma} = 0.067\ s^{-1}$), about 60% of the sample consisted of randomly oriented grains and 40% consisted of a single crystal with cylinder axes in the flow direction. The time scale for the formation of randomly oriented grains under shear flow was indistinguishable form that obtained under quiescent conditions. Under fast shear flow ($\dot{\gamma} = 0.67\ s^{-1}$), most of the sample (97%) was converted to a single crystal. To our knowledge, this study represents the first quantitative analysis of the unaligned grains that coexist with an aligned block copolymer microstructure. The present experiments constitute an extremely limited application of our theoretical model. Under many circumstances, one expects the unaligned grains to exhibit a nonrandom orientation distribution. This will result in depolarized scattering profiles with 2-fold symmetry. The analysis of such data will be presented in future publications.

Acknowledgment. We thank James Dai for his help with this project. Financial support from the National Science Foundation (CTS-9805852, and DMR-9901951), Research Corporation, and the Dreyfus Foundation to Polytechnic University is gratefully acknowledged. Acknowledgment is made to the donors of the Petroleum Research Fund, administered by the American Chemical Society, for support of this research.

Appendix

Expressions for $C(q)$ and $D(q)$. The expressions for $C(\mathbf{q})$ and $D(\mathbf{q})$ were obtained by substituting eq 22 into eq 16 and keeping terms up to order q_L^2

$$C(\mathbf{q}_T,q_L) = C(q_T,q_L) = \int_0^{\pi} d\theta_g \exp(-w^2 q_T^2/2) \sin^5\theta_g \times e^{-\zeta}((1 + \beta_1(\theta_g)q_L^2)I_0(\zeta) - \beta_2(\theta_g)q_L^2 I_1(\zeta)) \quad \text{(A1)}$$

and

$$D(\mathbf{q}_T,q_L) = D(q_T,q_L) = \int_0^{\pi} d\theta_g \exp(-w^2 q_T^2/2) \sin^5\theta_g\, e^{-\zeta}((1 + \beta_1(\theta_g)q_L^2)I_2(\zeta) - \beta_2(\theta_g)\theta_L^2 I_3(\zeta)) \quad \text{(A2)}$$

where $\zeta = {}^1/_2(q_T\Delta\sin\theta_g)$, $\Delta^2 = (l^2 - w^2)/4$, $\beta_1(\theta_g) = -(w^2/4) - \Delta^2 g_z^2 + \Delta^4 g_z^2 q_T^2 \sin^2\theta_g$, $\beta_2(\theta_g) = \Delta^4 g_z^2\, q_T^2 \sin^2\theta_g$, $g_z = \cos\theta_g$, and I_m is the modified Bessel function of order m.

References and Notes

(1) Strobl, G. *The Physics of Polymers*, 2nd ed.; Springer: New York, 1997.
(2) Chaikin, P. M.; Lubensky, T. C. *Principles of Condensed Matter Systems*; Cambridge: New York, 1995.
(3) Fuller, G. G. *Optical Rheometry of Complex Fluids*; Oxford: New York, 1995.
(4) Stein, R. S. *Polym. Lett.* **1971**, *9*, 747.
(5) Folkes, M. J.; Keller, A. *J. Polym. Sci., Polym. Phys. Ed.* **1976**, *14*, 833.
(6) Mattoussi, H.; Srinivasarao, M.; Kaatz, P. G.; Berry, G. C. *Macromolecules* **1992**, *25*, 2860.
(7) Newstein, M. C.; Garetz, B. A.; Balsara, N. P.; Chang, M. Y.; Dai, H. J. *Macromolecules* **1998**, *31*, 64.
(8) Wang, W.; Hashimoto, T. *Macromolecules* **1999**, *32*, 3163.
(9) Chen, Z. R.; Issaian, A. M.; Kornfield, J. A.; Smith, S. D.; Grothaus, J. T.; Satkowski, M. M. *Macromolecules* **1997**, *30*, 7096.
(10) Stein, R. S.; Erhardt, P. F.; Chu, W. *J. Polym. Sci., Part A-2* **1969**, *7*, 271.
(11) Chu, W.; Stein, R. S. *J. Polym. Sci., Part A-2* **1970**, *8*, 489.
(12) Burghardt, W. R. *Macromol. Chem. Phys.* **1998**, *199*, 471.
(13) Kannan, R.; Kornfield, J. A. *J. Rheol.* **1994**, *38*, 1127.
(14) Walker, L.; Wagner, N. *J. Rheol.* **1994**, *38*, 1525.
(15) Hadziioannou, G.; Skoulios, A. *Macromolecules* **1982**, *15*, 258.
(16) Koppi, K. A.; Tirrell, M.; Bates, F. S.; Almdal, K.; Colby, R. H. *J. Phys. (Fr.)* **1992**, *2*, 1941.
(17) Patel, S. S.; Larson, R.; Winey, K. I.; Watanabe, H. *Macromolecules* **1995**, *28*, 4313.

(18) Gupta, V. K.; Krishnamoorti, R.; Kornfield, J. A.; Smith, S. D. *Macromolecules* **1995**, *28*, 4464.
(19) Zhang, Y.; Weisner, U.; Yang, Y.; Pakula, T.; Speiss, H. W. *Macromolecules* **1996**, *29*, 5427.
(20) Balsara, N. P.; Hammouda, B. *Phys. Rev. Lett.* **1994**, *72*, 360.
(21) Balsara, N. P.; Hammouda, B.; Kesani, P. K.; Jonnalagadda, S. V.; Straty, G. C. *Macromolecules* **1994**, *27*, 2566.
(22) Almdal, K.; Bates, F. S.; Mortensen, K. *J. Chem. Phys.* **1992**, *96*, 9122.
(23) Morrison, F. A.; Mays, J. W.; Muthukumar, M.; Nakatani, A. I.; Han, C. C. *Macromolecules* **1993**, *26*, 5271.
(24) Balsara, N. P.; Dai, H. J.; Kesani, P. K.; Garetz, B. A.; Hammouda, B. *Macromolecules* **1994**, *27*, 7406.
(25) Balsara, N. P.; Dai, H. J. *J. Chem. Phys.* **1996**, *105*, 2942.
(26) Nakatani, A. I.; Morrison, F. A.; Douglas, J. F.; Mays, J. W.; Jackson, C. L.; Muthukumar, M.; Han, C. C. *J. Chem. Phys.* **1996**, *104*, 1589.
(27) Tepe, T.; Schulz, M. F.; Zhao, J.; Tirrell, M.; Bates, F. S. *Macromolecules* **1995**, *28*, 3008.
(28) Wang, H.; Kesani, P. K.; Balsara, N. P.; Hammouda, B. *Macromolecules* **1997**, *30*, 983.
(29) Wang, H.; Newstein, M. C.; Krishnan, A.; Balsara, N. P.; Garetz, B. A.; Hammouda, B.; Krishnamoorti, R. *Macromolecules* **1999**, *32*, 3695.
(30) Lin, L.; Argon, A. S. *J. Mater. Sci.* **1994**, *29*, 294.
(31) Donald, A. M.; Windle, A. H. *Liquid Crystalline Polymers*; Cambridge University Press: New York, 1992.
(32) Park, M.; Harrison, C.; Chakin, P. M.; Register, R. A.; Adamson, D. H. *Science* **1997**, *276*, 1401.
(33) Fink, Y.; Winn, J. N.; Fan, S.; Chen, C.; Michel, J. D.; Jonnapoulos, J. D.; Thomas, E. L. *Science* **1998**, *282*, 1679.
(34) Born, M.; Wolf, E. *Principles of Optics*, 5th ed.; Pergmon Press: Oxford, England, 1975.
(35) Nieto-Vesperinas, M. *Scattering and Diffraction in Physical Optics*; Wiley: New York, 1991.
(36) Balsara, N. P.; Garetz, B. A.; Dai, H. J. *Macromolecules* **1992**, *25*, 6072.
(37) The parameters l and w in this paper are identical to those defined in refs 7, 38, and 39, but smaller than those in ref 45 by a factor of $\sqrt{2}$. This difference arises from differences in the forms of the correlation functions used and affect the prefactor in eq 22.
(38) Garetz, B. A.; Newstein, M. C.; Dai, H. J.; Jonnalagadda, S. V.; Balsara, N. P. *Macromolecules* **1993**, *26*, 3151.
(39) Garetz, B. A.; Balsara, N. P.; Dai, H. J.; Wang, Z.; Newstein, M. C.; Majumdar, B. *Macromolecules* **1996**, *29*, 4675.
(40) Lin, C. C.; Jonnalagadda, S. V.; Kesani, P. K.; Dai, H. J.; Balsara, N. P. *Macromolecules* **1994**, *27*, 7769.
(41) Amundson, K. R.; Helfand, E.; Patel, S. S.; Quan, X.; Smith, S. S. *Macromolecules* **1992**, *25*, 1953.
(42) Balsara, N. P.; Perahia, D.; Safinya, C. R.; Tirrell, M.; Lodge, T. P. *Macromolecules* **1992**, *25*, 3896.
(43) Bates, F. S.; Schulz, M. F.; Khandpur, A. K.; Forster, S.; Rosedale, J. H.; Almdal, K.; Mortensen, K. *Faraday Discuss.* **1994**, *98*, 7.
(44) Wang, H. Ph.D. Thesis, Polytechnic University, 2000.
(45) Dai, H. J.; Balsara, N. P.; Garetz, B. A.; Newstein, M. C. *Phys. Rev. Lett.* **1996**, *77*, 3677.
(46) Balsara, N. P.; Garetz, B. A.; Newstein, M. C.; Bauer, B. J.; Prosa, T. J. *Macromolecules* **1998**, *31*, 7668.
(47) Lodge, T. P.; Fredrickson, G. H. *Macromolecules* **1992**, *25*, 5643.
(48) Laurer, J. H.; Pinherio, B. S.; Polis, D. L.; Winey, K. I. *Macromolecules* **1999**, *32*, 4999.
(49) Jager-Lezer, N.; Feutelais, Y.; Doucet, J.; Tranchant, J. F.; Alard, V.; Baszkin, A.; Grossiord, J. L. *J. Rheol.* **1999**, *43*, 1067.

MA991982Z